J Mol Model (2006) 12: 190–196
DOI 10.1007/s00894-005-0017-7

ORIGINAL PAPER

Jian-Guo Zhang · Qian Shu Li · Shao-Wen Zhang

The reaction of the aminoboranylidene-iminoborane isomerization: a CASSCF direct dynamics study

Received: 14 January 2005 / Accepted: 13 July 2005 / Published online: 18 August 2005

Abstract The barrier and the potential-energy surface of the isomerization from aminoboranylidene (BNH_2) to iminoborane (HBNH) have been studied using complete active space self-consistent field (CASSCF) with the 6−31 + G(d, p) basis set and higher-level energy methods. The rate constants of the isomerization reaction are reported by employing the direct *ab initio* dynamics method. The geometries of all the stationary points were optimized using the B3LYP and CCSD methods with the cc-pVTZ and cc-pVQZ basis sets. The information along the intrinsic reaction coordinate (IRC) was also calculated at the CASSCF/6−31 + G (d,p) level of theory. The energies were refined at the G3, G3MP2, G3MP2B3, CBS-Q, CBS-QB3, and two high-level (HL) methods based on the geometries optimized using CASSCF/6-31 + G(d,p). The rate constants were evaluated using conventional transition-state theory (TST), canonical variational transition-state theory (CVT), and canonical variational transition-state theory with small curvature tunneling correction (CVT/SCT) and conventional transition-state theory with Eckart tunneling correction (TST/Eckart). According to the calculated results, we conclude that the tunneling effect is very important to this isomerization reaction.

Keywords Isomerization · Aminoboranylidene (BNH_2) · Iminoborane (HBNH) · Ab initio calculation · CASSCF · Vibrational transition state theory · Rate constant

Introduction

Because the B-N pair is isoelectronic with C_2, a chemistry paralleling organic chemistry is to be expected, and many analogs have been synthesized and characterized. [1] In nature there appears to be a one-to-one correspondence between several structures of carbon and BN-allotropes, such as diamond [2] *vs.* cubic BN, [3] graphite *vs.* hexagonal BN, [4] benzene *vs.* borazine, [5, 6] fullerenes *vs.* BN-fullerenes, [7, 8, 9] and carbon nanotubes *vs.* BN nanotubes [10, 11] *etc.* However, the polarity of the B-N bond gives a somewhat different reactivity. Similarly, Westwood [12] reported a photoelectron study of aminoborane and found a correlation between its ionization potentials and those of ethylene. The formation of aminoborane from the ammonia-borane adduct has been studied by McKee [13] and Sakai, [14, 15] who find that the reaction is comparable to the dehydrogenation of ethane to yield ethylene.

This work focuses on the B-N analogy of the vinylidene-acetylene rearrangement, which has attracted the interest of both experimental [16, 17, 18] and theoretical [19, 20, 21, 22] chemists in the past. However, the lifetime and the existence of vinylidene are still a controversial problem. Early photodetachment spectra experiments [16] suggested vinylidene was metastable. However, more recently Coulomb-explosion experiments, [17] as well as theoretical simulations of the dynamics by Schork et al., [19] and by Hayes et al. [23] and Zou et al. [20, 24] have revealed significantly longer lifetimes. Higher-level *ab initio* calculations [20, 21, 25] have been used to determine the potential energy surfaces for several of these dynamics studies.

Lory [26] detected iminoborane by trapping it in an argon matrix, and later Kawashima et al. [27] detected iminoborane in the gas phase using diode laser IR spectroscopy. In 1995, Thompson et al. [28] gave an analysis of B-N products from laser ablation of boron in ammonia and reported vibrational bands in an argon matrix consistent with aminoboranylidene, and supported their assignments with CASSCF calculations. Paetzold [29] reviewed the chemistry of iminoborane. Reports of its experimental detection as well as of aminoboranylidene (BNH_2) and borylnitrene (H_2BN) are relatively scarce. The isomerization of borylnitrene to

J.-G. Zhang · Q. S. Li (✉) · S.-W. Zhang
State Key Laboratory of Explosion Science and Technology,
School of Science, Beijing Institute of Technology,
Beijing 100081, P. R. China
E-mail: qsli@bit.edu.cn
Fax: +86-10-68912665

iminoborane was studied using MP4 theory by Nguyen, [30] who identified the triplet state of borylnitrene as a minimum and the singlet state as a saddle point on the potential energy surface. Recently, the isomerization from aminoboranylidene to iminoborane was studied by Guo [13] using the MP2/6-31 + + G(d, p) level of theory, which gave the barrier for the reaction to be 28.67 kcal mol^{-1} and the heat of reaction to be −42.89 kcal mol^{-1}, although no substantive comparison to the available experimental data was reported. More recently, the singlet isomerization surface of aminoboranylidene to iminoborane was investigated by Rosas-Garcia [32] using coupled-cluster methods and large correlation consistent basis sets [CCSD(T)/cc-pVTZ], which gave the barrier to be 27.40 kcal mol^{-1} and the heat of reaction to be −41.35 kcal mol^{-1}.

In this work, we studied the structures of iminoborane, aminoboranylidene, and their transition states at many theoretical levels. Using the complete active space self-consistent field (CASSCF) method of theory, we have investigated the singlet isomerization surface of aminoboranylidene to iminoborane. In addition, in order to provide detailed dynamics information on the reaction and obtain the rate constants over a wide temperature range of the isomerization, high-level *ab initio* calculations and rate-constants calculations are still required. However, according to our knowledge, this paper is the first systematic attempt to study the directed dynamics on the isomerization reaction of aminoboranylidene to iminoborane.

Methodology

Electronic Structure Calculations

The geometries of all stationary points (reactants, products, and the transition state) are optimized using the B3LYP, CCSD and CASSCF methods with the cc-pVTZ, cc-pVQZ basis sets [33, 34, 35] and 6-31 + G(d, p) basis sets. [36, 37] Frequency analyses of all stationary points (reactants, products, and the transition state) were performed using B3LYP with the cc-pVTZ and cc-pVQZ basis sets and CASSCF method with the cc-pVTZ basis set. All stationary points (for reactant and product) had positive computed frequencies, while the transition states had only one imaginary frequency. Here, B3LYP [38] denotes the combination of the Becke's three-parameter exchange functional with the Lee-Yang-Parr (LYP) [39] correlation functional. CCSD [40, 41, 42] denotes the coupled cluster single- and double-excitation method. CASSCF [43, 44, 45, 46] indicates the complete active space self-consistent field energy calculations, in which full valence active spaces were used. In other words, the active space comprises all valence electrons in the all valence orbitals (the nitrogen 2*s*2*p* orbitals, the boron 2*s*2*p* orbitals, and the hydrogen 1 *s* orbitals) giving a CAS of ten electrons in ten active orbitals [CASSCF (10,10)]. To yield more reliable reaction enthalpies and barriers, the energies of all stationary points are further refined with several high level combination methods such as the G3, [47] G3MP2, [48] G3MP2B3, [49] CBS-Q, [50] CBS-QB3, [51, 52] and two combination methods [53, 54] (denoted as HL1 and HL2) based on the optimized geometries at the CASSCF/6-31 + G(d,p) level of theory. Here, the HL method employs a combination of quadratic configuration interaction calculations with perturbative inclusion of the triples contribution, QCISD(T), [42] and second-order Møller-Plesset perturbation theory (MP2). [55, 56] for the HL1, the 6-311G (d,p) basis set was used for the QCISD(T) calculations, and the 6-311 + + G(3df,2dp) basis set for the MP2 calculations. Also, the core electrons are treated as active in the MP2 evaluations for the latter basis set. Approximate QCISD (T, full)/6-311 + + G (3df, 2pd) estimates, E_{HL1}, were obtained as:

$$\begin{aligned} E_{\mathrm{HL1}} = {} & E[QCISD(T)/6-311G(d,p)] \\ & + E[MP2(full)/6-311++G(3df,2pd)] \\ & - E[MP2/6-311G(d,p)] \end{aligned}$$

The HL2 method estimates the infinite basis set limit *via* extrapolation of results obtained from sequences of correlation-consistent polarized-valence basis sets. The higher-level estimate, E_{HL2} is obtained as the sum of the QCISD(T) extrapolations. The combination of extrapolations can be expressed as: [53]

$$\begin{aligned} E_{HL2} = {} & E[QCISD(T)/cc-pVTZ] + \{E[QCISD(T)/cc-pVTZ] \\ & - E[QCISD(T)/cc-pVDZ]\} \times 0.46286 \\ & + E[MP2/cc-pVQZ] + \{E[MP2/cc-pVQZ] \\ & - E[MP2/cc-pVTZ]\} \times 0.69377 \\ & - E[MP2/cc-pVTZ] - \{E[MP2/cc-pVTZ] \\ & - E[MP2/cc-pVDZ]\} \times 0.46286 \end{aligned}$$

In order to reduce computational cost, the minimum energy path (MEP) was obtained using the intrinsic reaction coordinate (IRC) method [57] at the CAS (10,10)/6-31 + G (d, p) level of theory. In the calculation of rate constants, the energies of points on the MEP were refined with the HL1 and HL2 methods. All electronic structure calculations are carried out using the Gaussian 03 program. [58]

The rate Constant calculations

The rate constants were computed using conventional transition-state theory (TST), canonical variational transition-state theory (CVT), [59, 60] canonical variational transition-state theory with small curvature tunneling correction (CVT/SCT), [61] and the TST rate constant calculations with the Eckart tunneling correction (TST/Eckart) [62] using the online Vklab program package. [63]

In the present study, the reaction coordinate, s is defined as the distance along the MEP with the origin located at the saddle point and is negative on the reactant side and positive on the product side. For the canonical ensemble at a given temperature T, the canonical variational theory (CVT) thermal rate constant is given by

$$k^{CVT}(T) = \min_{s} k^{GT}(T,s)$$

where

$$k^{GT}(T,s) = \left\{ \sigma \frac{k_B T}{h} \frac{Q^{GT}(T,s)}{\Phi^R(T)} e^{-V_{MEP}(s)/k_B T} \right\}$$

where $k^{\mathrm{GT}}(T,s)$ is the generalized transition-state theory rate constant at the dividing surface that intersects the MEP at s and is orthogonal to the MEP at the intersection point. σ is the symmetry factor accounting for the possibility of more than one symmetry-related reaction path and can be calculated as the ratio of the product of the reactant rotational symmetry numbers to that of the transition state. k_{B} is Boltzman's constant and h is Plank's constant. Q^{GT} is the internal partition function of the generalized transition state with the local zero of energy at $V_{\mathrm{MEP}}(\mathrm{s})$, which is the classical potential energy along the minimum energy path s with its zero of energy at the reactants. Φ^R is the reactant partition function per unit volume for bimolecular reactions. Both the Q^{GT} and Φ^R are approximated as products of electronic, rotational, and vibrational partition functions. For Φ^R, the relative translational partition function is also included. Translational and rotational partition functions were evaluated classically whereas the vibrational partition functions were calculated quantum mechanically within the harmonic approximation for the present studies.

Furthermore, the CVT rate constants are corrected with the small-curvature tunneling (SCT) [64, 65] transmission coefficient. The SCT transmission coefficients, which include the reaction-path curvature effect on the transmission probability, were based on the centrifugal-dominant small curvature semi-classical adiabatic ground-state (CD-SCSAG) approximation. In particular, the transmission probability at energy E is given by

$$P(E) = \frac{1}{\{1 + e^{-2\theta(E)}\}}$$

where $\theta(E)$ is the imaginary action integral evaluated along the reaction coordinate

$$\theta(E) = \frac{2\pi}{h} \int_{s_l}^{sr} \sqrt{2\mu_{eff}(s)\left|E - V_a^G(s)\right|} ds$$

and where the integration limits s_l and s_r are the reaction-coordinate classical turning points. The reaction-path curvature effect on the tunneling probability is included in the effective reduced mass μ_{eff}.

Results and Discussion

Stationary Points

The optimized structures for the stationary points obtained at the CASSCF/6-31 + G(d,p) level of theory are given in Figure 1. Table 1 lists the optimized geometric parameters of the equilibrium and transition state of the reaction using the B3LYP, CCSD and CASSCF methods with the cc-pVTZ and cc-pVQZ basis sets along with the available experimental data. The optimized geometrical parameters of aminoboranylidene (BNH_2) and iminoborane (HBNH) at all the levels of theory employed are in good agreement with the available experimental values. [27] For the transition state, the predicted geometries also agree well between all the levels of theory. Comparing the results, we find that the structures agree well when using the same method with different basis sets. However, the results from CASSCF are larger than those of the other methods.

Table 2 abstracts the harmonic vibrational frequencies and zero-point energies of the equilibrium and transition-state structures of the reaction at the B3LYP

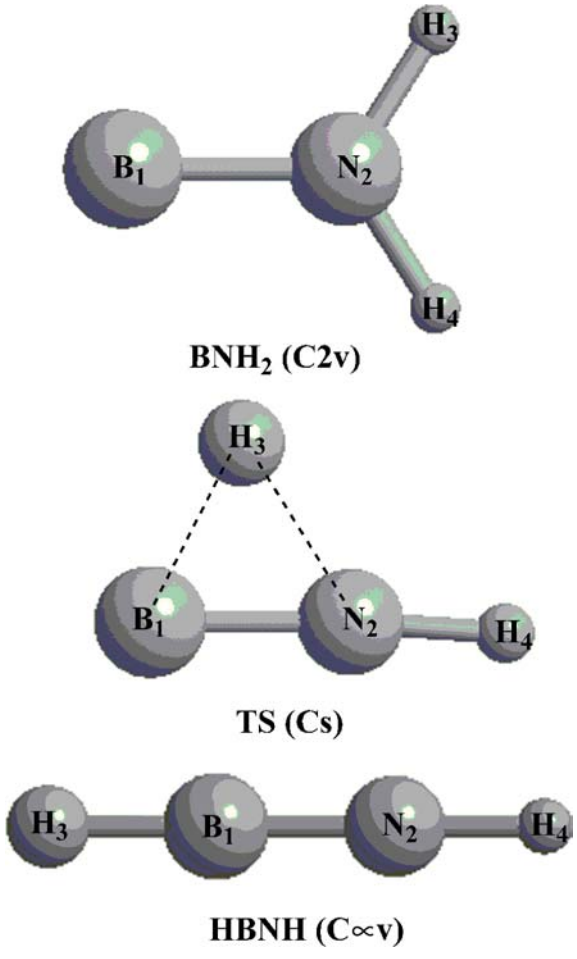

Fig. 1 Optimized geometries of the stationary points

Table 1 The optimized geometries of reactants, products and transition states using several methods with different basis sets

Species	Para[e]	B3LYP/TZ[a]	B3LYP/QZ[a]	CCSD/TZ[a]	CCSD/QZ[a]	CAS(10,10)/6–31 + g(d,p)	CAS(10,10)/TZ[a]	Reference[b]	Reference[c]	Exp.[d]
BNH_2 (C_{2v})	R(1,2)	1.373	1.371	1.376	1.376	1.403	1.396	1.348	1.376	
	R(2,3)	1.012	1.011	1.008	1.007	1.019	1.016	1.013	1.007	
	A(1,2,3)	122.8	122.8	122.8	122.7	122.5	122.5		122.7	
	A(3,2,4)	114.5	114.4			114.9	115.0	115.2		
TS (C_s)	R(1,2)	1.283	1.281	1.292	1.291	1.309	1.304	1.295	1.291	
	R(1,3)	1.307	1.306			1.327	1.322	1.309		
	R(2,4)	1.004	1.003	1.002	1.001	1.015	1.012	1.010	1.001	
	R(2,3)	1.398	1.396	1.389	1.389	1.403	1.412	1.386	1.389	
	A(2,1,3)	65.3	65.3			64.3	65.0	64.3	64.4	
	A(1,2,4)			176.4	176.3	175.8	176.0	174.6	176.3	
HBNH($C_{\infty v}$)	R(1,2)	1.234	1.232	1.238	1.237	1.252	1.247	1.247	1.237	1.238
	R(2,4)	0.991	0.991	0.988	0.989	1.001	0.998	0.996	0.989	
	R(1,3)	1.166	1.165	1.166	1.166	1.187	1.186	1.168	1.166	

[a]About the basis sets: cc-pVTZ and cc-pVQZ is abbreviated by TZ and QZ, respectively
[b]Reference [31] with MP2/6-311 + + G(d,p) method of theory
[c]Reference [32] with CCSD(T)/cc-pVQZ method of theory
[d]Reference [27]
[e]Bond lengths in Å and bond angles in deg

and CASSCF levels of the theory with different basis sets along with the previously calculated results [31, 32] and the available experimental data. [27] From the data, we find that the calculated frequencies are quite scattered, both for the different methods and compared with the previous calculated results. [31, 32] However, the same method (B3LYP or CASSCF) with different basis sets (cc-pVTZ, cc-pVTZ or 6-31 + G(d,p) provide good prediction of frequencies for all modes. As for the imaginary frequency of the transition state, the theoretical predictions are also quite scattered. The predicted values of the imaginary frequency are 1451*i*, 1447*i*, 1877*i*, and 1748*i* cm^{-1} at the B3LYP/cc-pVTZ, B3LYP/cc-pVQZ, CAS(10,10)/6-31 + g(d,p) and CAS(10,10)/cc-

Table 2 Harmonic Frequencies (cm^{-1}), the code and integers in parentheses are the Symmetry and Infrared Intensities (km mol^{-1}) and zero-point energies (kcal mol^{-1}) for the reactants, products and transition states using several methods with difference basis sets

Species	**Methods**	**Harmonic Frequencies (cm^{-1}) and Infrared Intensities (km mol^{-1})**	**ZEP**
$BNH_2(C_{2v})$	B3LYP/cc-pVTZ	431(B1,166), 614(B2,9), 1267(A1,37), 1568(A1,180), 3523(A1,43), 3627(B2,80)	15.77
	B3LYP/cc-pVQZ	434(B1,163), 616(B2,9), 1266(A1,40), 1569(A1,188), 3520(A1,44), 3622(B2,82)	15.76
	CAS(10,10)/6-31 + g(d,p)	494(B1,233), 682(B2,4), 1230(A1,86), 1620(A1,166), 3520(A1,62), 3640(B2,69)	15.99
	CAS(10,10)/cc-pVTZ	457(B1,181), 675(B2,8), 1247(A1,71), 1610(A1,135), 3498(A1,61), 3612(B2,65)	15.87
	[a]Reference [MP2/6-311 + + G(d,p)]	316, 583, 1251, 1565, 3576, 3697	15.71
	[b]Reference [CCSD(T)/cc-pVQZ]	430(172), 613(9), 1271(53), 1579(178), 3566(58), 3678(78)	
	[c]Exp.	596, 1533	
$TS(C_s)$ [d]	B3LYP/cc-pVTZ	1451*i*(*A'*,471), 204(*A''*,158), 817(*A'*,106), 1636(*A'*,67), 2229(*A'*,67), 3692(*A'*,116)	12.26
	B3LYP/cc-pVQZ	1447*i*(*A'*,486), 209(*A''*,154), 818(*A'*,104), 1640(*A'*,69), 2230(*A'*,68), 3694(*A'*,118)	12.28
	CAS(10,10)/6-31 + g(d,p)	1877*i*(*A'*,713), 287(*A''*,189), 832(*A'*,119), 1561(*A'*,83), 2149(*A'*,34), 3652(*A'*,122)	12.12
	CAS(10,10)/cc-pVTZ	1748*i*(*A'*,628), 253(*A''*,160), 814(*A'*,98), 1563(*A'*,69), 2149(*A'*,48), 3626(*A'*,120)	12.02
	[a] Reference [MP2/6-311 + + G(d,p)]	1679*i*, 306, 805, 1621, 2302, 3706	12.49
	[b] Reference [CCSD(T)/cc-pVTZ]	1592*i*(594), 372(157), 839(104), 1608(64), 22242(57), 3733(113)	
HBNH($C_{\infty v}$)	B3LYP/cc-pVTZ	473×2(π,122), 742×2(π,0), 1844(σ,45), 2884(σ,12), 3874(σ,197)	15.77
	B3LYP/cc-pVQZ	478×2(π,119), 744×2(π,0), 1845(σ,50), 2886(σ,14), 3869(σ,197)	15.79
	CAS(10,10)/6-31 + g(d,p)	528×2(π,138), 737×2(π,1), 1802(σ,36), 2795(σ,27), 3836(σ,190)	15.67
	CAS(10,10)/cc-pVTZ	506×2(π,113), 730×2(π,1), 1780(σ,28), 2771(σ,28), 3798(σ,186)	15.50
	[a]Reference [MP2/6-311 + + G(d,p)]	456×2, 741×2, 1793, 2915, 3889	15.71
	[b]Reference [CCSD(T)/cc-pVQZ]	488(113), 732(1), 1821(33), 2888(11), 3887(186)	
	[c]Exp.	462, 464, 678, 683, 1819, 2796, 3712	

[a]Reference [31],
[b]Reference [32],
[c]Reference [28]
[d]here is only an image frequency (showed in the table in bold, italic, and underline style) for TS.
[e]Reference [66]

pVTZ levels of theory, respectively. The difference in the imaginary frequency is caused by the different shapes of the minimum energy paths (MEP) near the transition state among the methods. Since CAS(10,10)/6-31 + g(d,p) provides the largest imaginary frequencies, we employed the results for the TS and IRC calculations from CAS(10,10)/6-31 + g(d,p) in this paper.

Table 3 shows the reaction energies (ΔE), the classical potential barriers ($V^{\neq}$), the vibrational adiabatic ground-state potential ($V_a^{G\neq}$), reaction enthalpies (ΔH_{298K}°) and the reaction free energies (ΔG_{298K}°) with different methods and the previous theoretical results. [31, 32] The predicted values of these properties are quite consistent at the same method with different basis sets. However, they are quite scattered among different methods. The values of ΔE, $V^{\neq}$, $V_a^{G\neq}$, ΔH_{298K}° and ΔG_{298K}° are −41.31, 30.52, 27.01, −41.45, and −40.59 kcal mol^{-1} at the B3LYP/cc-pVTZ level of theory, respectively, which is in agreement with previous calculated results of ΔE and $V_a^{G\neq}$ to be −41.35 and 27.40 kcal mol^{-1} by Rosas-Garcia [32] using CCSD(T)/cc-pVTZ. When we refine these energies using different methods based on the CAS(10,10)/6-31 + g(d,p) geometry, the values of each property are relatively close. And the values of potential barriers ($V_a^{G\neq}$) from the higher-level methods agree with previous calculated results by Rosas-Garcia [32] and Guo. [31] This means that the optimized structures based on the CAS(10,10)/6-31 + g(d,p) level of theory are relative reliable.

Reaction Path Properties

The minimum-energy paths were obtained using the intrinsic reaction coordinate (IRC) theory at the CAS(10,10)/6-31 + g(d,p) level of theory and the potential energy profiles were further refined at the HL_1 and HL_2 levels. Figure 2 depicts the vibrationally adiabatic ground-state potential energy curves (V_a^G) of the reaction as a function of s (amu)$^{1/2}$ bohr using the refined energies from the HL_1 and HL_2 methods based on the CAS(10,10)/6-31 + g(d,p) level of theory using the interpolated method. It can be seen that for the reaction the V_a^G curve at this level is an ideal potential surface. It can be seen that the V_a^G curve at the HL1// CAS(10,10)/6-31 + g(d,p) level is close to that at the HL2// CAS(10,10)/6-31 + g(d,p) level of theory.

Rate constant calculations

We calculated the rate constants using the CVT, CVT/ZCT, CVT/SCT, TST, and TST/Eckart methods based on the interpolated MEP at the HL1//CAS(10,10)/6-31 + g(d,p) and HL2//CAS(10,10)/6-31 + g(d,p) levels of theory. The quantum tunneling effects are included in the rate constant calculations with the Eckart tunneling model. The rate constants are shown in Figures 3 and 4. It is obvious that the vibrational and tunneling effects are very important at low temperatures. At 200 K, the rate constant of TST/Eckart to be the largest is 2.60×10^{-7} s^{-1} and 1.31×10^{-7} s^{-1} at the HL1//CAS(10,10)/6-31 + g(d,p) and HL2//CAS(10,10)/6-31 + g(d,p) levels of theory, respectively. The A value, the so-called pre-exponential factor from the CVT/ZCT method is about 10^{-13} s^{-1}, which is agreement with Guo's result. [31] The rate constants of CVT/SCT and CVT/ZCT are larger than those of CVT by a factor of 10^{10}, so we conclude that the tunneling effect is very important in this isomerization reaction. However, the rate constants of all methods become almost identical as the temperature increases above 1000 K. The rate constants of TST/Eckart and CVT/SCT

Table 3 The reaction energetic parameters (kcal mol^{-1}) at different levels of theory

Method	E	$V^{\neq}$	$V_a^{G\neq}$	H_{298K}^0	G_{298K}^0
B3LYP/cc-pVTZ	−41.31	30.52	27.01	−41.45	−40.59
B3LYP/cc-pVQZ	−41.54	30.32	26.84	−41.67	−40.80
CCSD(T)/cc-pVQZ//CAS(10,10)/6-31 + G(d,p)	−38.51	31.87	27.90	−38.97	−38.10
QCISD(T)/cc-pVQZ//CAS(10,10)/6-31 + G(d,p)	−38.73	31.65	27.68	−39.19	−38.32
QCISD(T)/cc-pVTZ//CAS(10,10)/6-31 + G(d,p)	−37.92	32.03	28.16	−38.38	−37.50
QCISD(t)/6-311g(d,p)//CAS(10,10)/6-31 + G(d,p)	−38.05	32.51	28.64	−40.18	−39.30
MP2/cc-pVTZ//CAS(10,10)/6-31 + G(d,p)	−43.62	30.85	26.98	−44.08	−43.20
MP2/cc-pVQZ//CAS(10,10)/6-31 + G(d,p)	−44.41	30.47	26.61	−44.87	−44.00
MP2/6-311g(d,p)//CAS(10,10)/6-31 + G(d,p)	−43.71	31.49	27.62	−38.51	−37.63
MP2(Full)/6-311 + + g(3df,2pd)//CAS(10,10)/6-31 + G(d,p)	−45.38	30.02	26.16	−39.84	−38.97
E_{HL1}//CAS(10,10)/6-31 + G(d,p)	−39.71	31.05	27.18	−45.84	−44.97
E_{HL2}//CAS(10,10)/6-31 + G(d,p)	−39.38	31.44	27.57	−44.18	−43.30
G3	−39.21			−39.68	−38.80
G3MP2	−38.32			−38.78	−37.91
G3MP2B3	−38.26			−38.72	−37.84
CBS-Q	−39.62			−40.09	−39.21
CBS-QB3	−39.36			−39.82	−38.95
Reference[a] [MP2/6-311 + + G(d,p)]	−42.89		28.67	−43.12	−42.14
Reference[b] [CCSD(T)/cc-pVTZ]	−41.35		27.40		

[a]Reference [31]
[b]Reference [32]

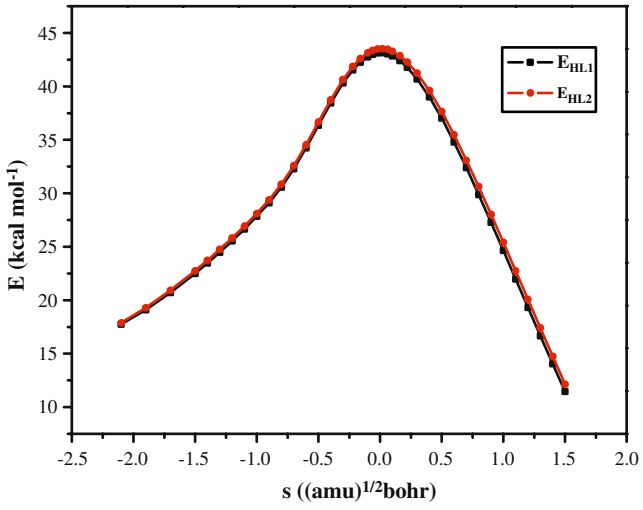

Fig. 2 The vibrationally adiabatic ground-state potential energy curves (V_a^G) of the reaction as a function of s (amu)$^{1/2}$ bohr at the HL1// CASSCF/6-31 + G(d,p) and HL2//CASSCF/6-31 + G(d,p) levels of theory

are higher than those of CVT/ZCT and the rate constants of CVT are very similar with those of TST in the whole temperature range. The TST rate constant shows a similar trend to Guo's previous TST data [31] using the MP2/6-3111 + + G (d, p) method of theory. The fitted rate expression calculated from the CVT/SCT method using the interpolated CAS (10,10)/6-31 + g (d, p) MEP with refined energies from the HL1 and HL2 methods are $k(T) = 1.91 \times 10^{-19} \times T^{9.37} \times e^{(5.26\times10^3/T)}\mathrm{s}^{-1}$ and $k(T) = 1.64 \times 10^{-19} \times T^{9.39} \times e^{(5.47\times10^3/T)}\mathrm{s}^{-1}$ in the temperature range 200-2500 K, respectively. We can find that the rate constants from the CVT/SCT method are very consistent with each other using the HL1 and HL2 methods.

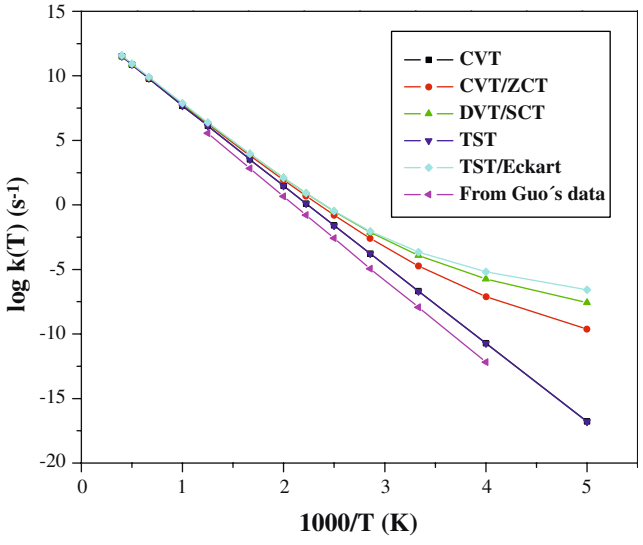

Fig. 3 Arrhenius plot of the rate constants calculated at the CVT, CVT/ZCT, CVT/SCT, TST and TST/Eckart levels of theory. The rate constants are calculated based on the interpolated MEP at the HL1//CASSCF/6-31 + G(d,p) level of theory

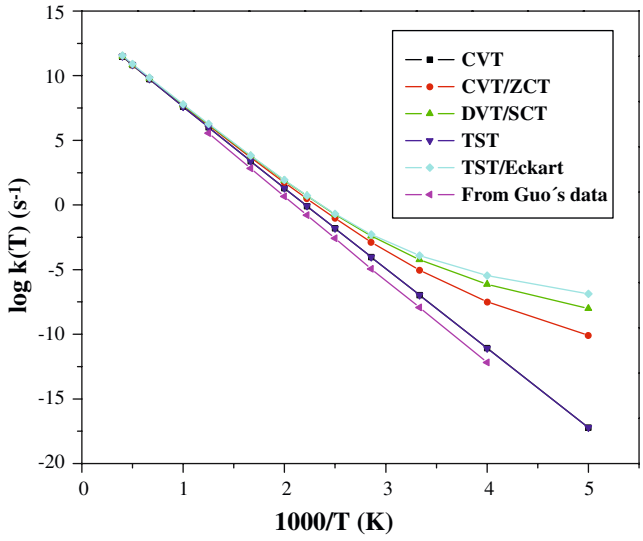

Fig. 4 Arrhenius plot of the rate constants calculated at the CVT, CVT/ZCT, CVT/SCT, TST and TST/Eckart levels of theory. The rate constants are calculated based on the interpolated MEP at the HL2//CASSCF/6-31 + G(d,p) level of theory

Summary

In the present study, we present a direct *ab initio* dynamics study of the thermal rate constants of the unimolecular isomerization reaction of $BNH_2 \rightarrow$ HBNH. B3LYP/cc-pVT (Q) Z, CCSD/cc-pVT (Q) Z, and CAS (10,10)/6-31 + G (d, p) levels of theories were employed to optimize the geometries of all stationary points. The minimum energy path (MEP) was given using CAS (10,10)/6-31 + G (d, p). The energies of all the stationary points were refined at a series of higher-level methods including HL1, HL2, and QCISD (T)/aug-cc-pVTZ levels of theory. The rate constants were evaluated based on the energetics from the HL1//CAS (10,10)/6-31 + G (d, p) and HL2//CAS (10,10)/6-31 + G (d, p) levels of theory using conventional transition-state theory (TST), canonical variational transition-state theory (CVT), and canonical variational transition-state theory with small curvature tunneling correction (CVT/SCT) and conventional transition-state theory with Eckart tunneling correction (TST/Eckart) in the temperature range of 200–2500 K. According to the calculated results, we can conclude that the tunneling effect is very important in this isomerization reaction, particularly in the low temperature region. The fitted three-parameter Arrhenius expression from the CVT/SCT rate constants from the HL1 and HL2 method are $k(T) = 1.91 \times 10^{-19} \times T^{9.37} \times e^{(5.26\times10^3/T)}\mathrm{s}^{-1}$ and $k(T) = 1.64\times10^{-19} \times T^{9.39} \times e^{(5.47\times10^3/T)}\mathrm{s}^{-1}$ in the temperature range 200–2500 K, respectively. We find that the rate constant from CVT/SCT method is very consistent with each other for the HL1 and HL2 method.

Acknowledgement Our thanks are due to D.G. Truhlar for providing the POLYRATE 8.2 program. This work was supported by

the National Natural Science Foundation of China (No. 20373007 and No. 20471008) and the Foundation for basic research by the Beijing Institute of Technology.

References

1. Pusatcioglu SY, Mc-Gee Jr HA, Fricke AL, Hassler JC (1977) J Appl Polym Sci 21:1561–1562
2. Manaa MR (2001) J Mol Struct (Theochem) 549:23–26
3. Solozhenko VL, Will G, Hupen H, Elf F (1994) Solid State Commun 90:65–67
4. Edgar JH (1992) J Mater Res 7:235–256
5. Lazzeretti P, Tossell JA (1991) J Mol Struct (Theochem) 236:403–410
6. Boese R, Maulitz AH, Stellberg P (1994) Chem Ber 127:1887–1889
7. Alexandre SS, Chacham H, Nunes RW (2001) Phys Rev B 63:045402/1–04502/5
8. Hirano T, Oku T, Suganuma K (2000) Diamond and Relat Mater 9:625–628
9. Pokropovny VV, Skorokhod VV, Olieinik GS, Kurdyumov AV (2000) J Solid State Chem 154:214–222
10. Deepak FL, Vinod CP, Mukhopadhyay K, Govindaraj A, Rao CNR (2002) Chem Phys Lett 353:345–352
11. Kongsted J, Osted A, Jensen L, Astrand PO, Mikkelsen KV (2001) J Phys Chem B 105:10243–10248
12. Westwood NPC, Werstiuk NH (1986) J Am Chem Soc 108:891–894
13. McKee ML (1992) J Chem Phys 96:5380–5385
14. Sakai S (1995) J Phys Chem 99:5883–5888
15. Sakai S (1994) Chem Phys Lett. 217:288–292
16. Erwin KM, Ho J, Lineberger WC (1989) J Chem Phys 91:5974–5992
17. Levin J, Feldman H, Baer A, Ben-Hamu D, Heber O, Zajfman D, Vager Z (1998) Phys Rev Lett 81:3347–3350
18. Jacobson MP, Field RW (2000) J Phys Chem A 104:3073–3086
19. Schork R, Koppel H (2001) J Chem Phys 115:7907–7923
20. Zou S, Bowman JM (2003) Chem Phys Lett 368:421–424
21. Stanton JF, Gauss J (1999) J Chem Phys 110:6079–6080
22. Zou S, Bowman JM (2002) J Chem Phys 116:6667–6673
23. Hayes RL, Fattal E, Govind N, Carter EA (2001) J Am Chem Soc 123:641–657
24. Zou S, Bowman JM, Brown A (2003) J Chem Phys 118:10012–10023
25. Chang N-Y, Shen M-Y, Yu C-H (1997) J Chem Phys 106:3237–3242
26. Lory ER, Porter RF (1973) J Am Chem Soc 95:1766–1770
27. Kawashima Y, Kawaguchi K, Hirota E (1987) J Chem Phys 87:6331–6333
28. Thompson CA, Andrews L, Martin JML, El-Yazal J (1995) J Phys Chem 99:13839–13849
29. Paetzold P (1991) Pure & Appl Chem 63:345–350
30. Nguyen MT (1987) J Chem Soc, Chem Commun: 342–344
31. Guo Z-C (2001) Chinese J Struct Chem 20:396–398
32. Rosas-Garcia VM, Crawford TD (2003) J Chem Phys 119:10647–10652
33. Dunning Jr TH (1989) J Chem Phys 90:1007–1023
34. Kendall RA, Dunning Jr TH, Harrison RJ (1992) J Chem Phys 96:6796–6806
35. Woon DE, Dunning Jr TH (1993) J Chem Phys 98:1358–1371
36. Frisch M, Pople JA, Binkley JS (1984) J Chem Phys 80:3265–3269
37. Francl MM, Pietro WJ, Hehre WJ, Binkley JS, Gordon MS, DeFrees DJ, Pople JA (1982) J Chem Phys 77:3654–3665
38. Becke AD (1996) J Chem Phys 104:1040–1046
39. Lee C, Yang W, Parr RG (1988) Phys Rev B 37:785–789
40. Bartlett RJ (1989) J Phys Chem 93:1697–1708
41. Scuseria GE, Schaefer III HF (1989) J Chem Phys 90:3700–3703
42. Pople JA, Head-Gordon M, Raghavachari K (1987) J Chem Phys 87:5968–5975
43. Cullen J (1999) J Comput Chem 20:999–1008
44. Yamamoto N, Vreven T, Robb MA, Frisch MJ, Schlegel HB (1996) Chem Phys Lett 250:373–378
45. Frisch MJ, Ragazos IN, Robb MA, Schlegel HB (1992) Chem Phys Lett 189:524–528
46. Malmqvist PA, Roos BO (1989) Chem Phys Lett 155:189–194
47. Curtiss LA, Raghavachari K, Redfern PC, Rassolov V, Pople JA (1998) J Chem Phys 109:7764–7776
48. Curtiss LA, Redfern PC, Raghavachari K, Rassolov V, Pople JA (1999) J Chem Phys 110:4703–4709
49. Baboul AG, Curtiss LA, Redfern PC, Raghavachari K (1999) J Chem Phys 110:7650–7657
50. Ochterski JW, Petersson GA, Montgomery JA (1996) J Chem Phys 104:2598–2619
51. Montgomery JA, Frisch MJ, Ochterski JW, Petersson GA (1999) J Chem Phys 110:2822–2827
52. Montgomery JA, Frisch MJ, Ochterski JW, Petersson GA (2000) J Chem Phys 112:6532–6542
53. Miller JA, Klippenstein SJ (2003) J Phys Chem A 107:2680–2692
54. Martin JML (1996) Chem Phys Lett 256:669–674
55. Frisch MJ, Head-Gordon M, Pople JA (1990) Chem Phys Lett 166:275–280
56. Head-Gordon M, Pople JA, Frisch MJ (1988) Chem Phys Lett 153:503–506
57. Gonzalez C, Schlegel HB (1989) J Chem Phys 90:2154–2161
58. Frisch MJ, Trucks GW, Schlegel HB, Scuseria GE, Robb MA, Cheeseman JR, Montgomery J, J.A., Vreven T, Kudin KN, Burant JC, Millam JM, Iyengar SS, Tomasi J, Barone V, Mennucci B, Cossi M, Scalmani G, Rega N, Petersson GA, Nakatsuji H, Hada M, Ehara M, Toyota K, Fukuda R, Hasegawa J, Ishida M, Nakajima T, Honda Y, Kitao O, Nakai H, Klene M, Li X, Knox JE, Hratchian HP, Cross JB, Adamo C, Jaramillo J, Gomperts R, Stratmann RE, Yazyev O, Austin AJ, Cammi R, Pomelli C, Ochterski JW, Ayala PY, Morokuma K, Voth GA, Salvador P, Dannenberg JJ, Zakrzewski VG, Dapprich S, Daniels AD, Strain MC, Farkas O, Malick DK, Rabuck AD, Raghavachari K, Foresman JB, Ortiz JV, Cui Q, Baboul AG, Clifford S, Cioslowski J, Stefanov BB, Liu G, Liashenko A, Piskorz P, Komaromi I, Martin RL, Fox DJ, Keith T, Al-Laham MA, Peng CY, Nanayakkara A, Challacombe M, Gill PMW, Johnson B, Chen W, Wong MW, Gonzalez C, Pople JA (2003) Gaussian 03. Gaussian Inc, Pittsburgh PA
59. Truhlar DG, Fast PL (1998) J Chem Phys 109:3721–3729
60. Truong NT (1994) J Chem Phys 100:8014–8025
61. Liu Y-P, Lynch GC, Troung TN, Lu D-H, Truhlar DG, Garrett BC (1993) J Am Chem Soc 115:2408–2415
62. Baer T, Hase WL (1996) Unimolecular Reaction Dynamics (International Series of Monographs on Chemistry). Oxford University Press, New York
63. Zhang S-W, Truong TN (2001) VKLab version 1.0. University of Utah
64. Truhlar DG, Isaacson AD, Garrett BC (1985) Boca Raton, FL CRC
65. Steckler R, Hu W-P, Liu Y-P, Lynch GC, Garret BC, Isaacson AD, Melissas VS, Lu D-H, Troung TN, Rai SN, Hancock GC, Lauderdale JG, Joseph T, Truhlar DG (1995) Comput Phys Commun 88:341–343
66. Brint P, Sangchakr B, Fowler PW (1989) J Chem Soc Faraday Trans II 85:29–37